

Mex3a-dependent post-transcriptional silencing assures olfactory receptor diversity and axon guidance specificity

Rachel Duffié¹, Hani Shayya¹, Martín Escamilla del Arenal¹, Miao Wang¹, Jerome Kahiapo¹, Fiona Clowney¹, Aileen Ugurbil¹, Abdurrahman Keskin², Elizaveta V. Bashkirova¹, Ariel D. Pourmorady¹, Ira Schieren¹, Humberto Ibarra Avila¹, Francisco M. Barriga^{3,4}, Eduard Batlle^{4,5,6}, Marko Jovanovic², Stavros Lomvardas^{1,7}

1. Mortimer B. Zuckerman Mind, Brain, and Behavior Institute, Columbia University New York, NY 10027, USA
2. Department of Biological Sciences, Columbia University, New York, NY 10027, USA
3. Systems Oncology Program, Vall d'Hebron Institute of Oncology (VHIO), Vall d'Hebron Barcelona Hospital Campus, 08035, Barcelona, Spain
4. Institute for Research in Biomedicine (IRB Barcelona), The Barcelona Institute of Science and Technology (BIST), Baldiri i Reixac 10, 08028 Barcelona, Spain
5. Centro de Investigación Biomédica en Red de Cáncer (CIBERONC), Barcelona, Spain.
6. Institució Catalana de Recerca i Estudis Avançats (ICREA), Barcelona, Spain.
7. Department of Biochemistry and Molecular Biophysics, Vagelos College of Physicians and Surgeons, New York, NY 10032, USA

Abstract

Olfactory sensory neurons (OSNs) use olfactory receptor (OR)-specific patterns of ER stress to transform OR sequence identity into axon guidance precision. However, during neuronal differentiation, OSNs transiently co-express random combinations of OR genes, which could generate unpredictable ER stress signatures that are not conducive to axon guidance precision. Here, we show that post-transcriptional OR silencing by the transiently expressed and exclusively cytoplasmic RING and KH domain protein Mex3a, decouples OR transcription from OR protein induced ER stress, until the developmental onset of singular OR transcription. Consequently, conditional Mex3a deletion results in premature induction of ER stress during the polygenic stage of OR transcription, which biases OR gene choice towards the OR alleles that are transcribed first and perturbs the specificity of OR-regulated axon targeting, disrupting the glomerular map of odor representation in the olfactory bulb. Our experiments reveal the critical role of post-transcriptional gene regulation in a fundamental cellular pathway that influences the assembly of neuronal circuits.

Introduction

Vertebrate olfactory systems are governed by the “one receptor per neuron” and the “one receptor per glomerulus” principles that transform singular OR gene choice into axon guidance specificity. OR DNA, mRNA, and protein sequences contain regulatory information that enables both governing principles: OR DNA CDSs promote their own transcriptional silencing¹; OR mRNAs enforce transition from polygenic to singular OR transcription²; OR proteins stabilize OR gene choice³⁻⁶, promote OSN differentiation³, and instruct OSN axon guidance specificity⁷⁻⁹. While OR DNA and nascent OR RNA act in the nucleus, inducing heterochromatic silencing^{10,11}, genomic compartmentalization^{12,13}, and assembly of multi-chromosomal enhancer hubs¹⁴⁻²⁰, OR protein elicits its regulatory function through the ER, via Perk induction and eIF2a phosphorylation³. Any level of Perk induction upon a threshold suffices for Atf5 translation and stabilization of singular OR choice^{3,21}. OR sequence-dependent variations of Perk signaling, on the other hand, determine axon targeting specificity through Ddit3-dependent regulation of axon guidance genes⁷. Thus, quantitative differences in Perk induction⁷, together with the distinct activity properties of each OR^{22,23}, transform stochastic OR gene choice into a stereotypic map of OR representation in the brain.

Any process that leverages the identity of the OR protein to instruct axon guidance precision should rely on singular OR expression, or invariant OR co-expression between OSNs that project to the same glomerulus. Yet, immediate neuronal precursors (INPs) and early immature OSNs (iOSNs) co-transcribe diverse repertoires of OR genes^{18,20,24,25}. Thus, neither Perk signaling⁷, nor neuronal activity^{22,23} can fine-tune axon guidance in differentiating OSNs, as these will be significantly variable between cells that eventually choose the same OR. Indeed, even though Atf5 is highly transcribed at the earliest stage of OSN differentiation, Perk-dependent Atf5 translation coincides with the transition to singular OR transcription. Thus, a post-transcriptional mechanism must prevent co-transcribed ORs from inducing Perk signaling, to insulate OSN axon guidance from OR protein identity until the transition to transcriptional singularity is complete. On this note, it was previously proposed that unique features of the 5' and 3' untranslated sequences (UTR) may subject the OR superfamily to post-transcriptional regulation²⁶, while more recently it was shown that mutations in components of the mRNA decay pathway alter the OR repertoire expressed in the mutant MOEs²⁷. A direct demonstration of post-transcriptional OR silencing in the developing MOE, however, has yet to be shown.

Here, we identify Mex3 RNA-binding family member A (Mex3a), a KH and RING domain-containing protein²⁸ as a post-transcriptional repressor of OR expression. We show that Mex3a interacts with several RNA binding proteins involved in post-transcriptional silencing, mRNA stability, and translational inhibition, and we reveal that the OR CDS is sufficient for this silencing. We show that efficient OR silencing is dependent upon an intact Mex3a RING domain, suggesting a pleiotropic role of Mex3a in OR silencing that could reduce OR mRNA stability, OR mRNA translation, and, possibly, OR protein stability. While our gain of function experiments demonstrate the ability of Mex3a to silence ORs in mature OSNs (mOSNs), loss of function experiments propose that the endogenous Mex3a protein promotes post-transcriptional OR silencing in INPs and iOSNs, reducing Perk signaling during the polygenic and oligogenic phases of OR transcription. Consequently, Mex3a deletion causes heterochronic induction of the OR protein feedback which could enable co-transcribed ORs to influence axon guidance. The former alters OR gene choice patterns in the main olfactory epithelium (MOE), while the latter perturbs

the precision by which like axons converge to distinct glomeruli in the olfactory bulb (OB). Therefore, our experiments uncover a novel, post-transcriptional layer of OR gene regulation, demonstrate its importance for the diversification and wiring of olfactory neurons, and propose novel regulatory roles for Mex3a.

Mex3a silences OR expression in olfactory neurons

We hypothesized that polygenic OR transcription cannot elicit OR protein feedback or influence OSN axon guidance. OR transcription could be decoupled from OR protein expression if OR mRNA trafficking to the cytoplasm were impaired; if OR mRNA stability were reduced; or if OR mRNA translation were inhibited. We compared single nucleus (sn) and single cell (sc) RNA-seq experiments to ask if any of these processes operate in the MOE. Consistent with previous reports, scRNA-seq shows a strong increase in OR mRNA abundance from polygenic (INPs), to oligogenic (iOSNs), and eventually monogenic (mOSNs) stages of OR transcription. In contrast, snRNA-seq detects similar amounts of total nuclear OR RNA between INPs and iOSNs, and only a small increase in mOSNs (Fig. 1a). Moreover, bulk RNA-seq experiments from FAC-sorted cells from the MOE reveal that the intron/exon ratio of total OR reads is highest in INP cells and decreases with differentiation (Extended Data Fig. 1a). Taken together, these observations raise the exciting possibility that OR mRNA stability is reduced in INPs, and less so in iOSNs, compared to mOSNs. We therefore searched for post-transcriptional silencers with strong expression in INPs that are reduced in iOSNs and turned off in mOSNs. Post-transcriptional repressor Mex3a, one of 4 highly homologous RNA binding proteins²⁸, exhibits this pattern, as it has highest mRNA expression in INPs that declines in iOSNs and is absent in mOSNs (Fig. 1b). Immunofluorescence (IF) experiments confirm that Mex3a protein is abundant in the cytoplasm of OSN progenitors and iOSNs but undetectable in Vglut2-expressing mOSNs (Fig. 1c).

At physiological levels Mex3a promotes renewal and maintenance of intestinal^{29,30} and neuronal stem cells^{31,32}, while ectopic Mex3a expression in cancers is associated with poor prognosis³³. Mex3a expression in the MOE, which persists in post-mitotic iOSNs, is not consistent with a simple role in stem cell maintenance. Reasoning that Mex3a downregulation in mOSNs is essential for OR expression, we sought to restore Mex3a expression in these terminally differentiated neurons. To achieve this, we generated a tTA-inducible Mex3a transgene (tetO-Mex3a-t2a-mCherry, referred to as Mex3a Tg throughout), which we crossed to an OMP-IRES-tTA driver³⁴ (termed OMP-tTA) (Fig. 1d). RNA-seq analysis comparing FAC-sorted OSNs that express the Mex3a Tg vs tetO-GFP³⁵ (referred to as GFP Tg), revealed widespread downregulation for most OR genes, 42% of which are significantly downregulated (Fig. 1e). In aggregate, we find a significant reduction of all the OR mRNAs in Mex3a Tg mOSNs, which is not observed for the rest of the mOSN transcriptome (Fig. 1f). On this note, we have previously shown that OR expression influences the expression of numerous mOSN markers^{3,7}, thus, transcriptional changes that give Mex3a-expressing OSNs a less differentiated signature (Extended Data Fig. 1b), may be a direct consequence of OR downregulation. IF with antibodies that detect OR proteins Mor28 (Olfr1507), C6 (Olfr49), M71 (Olfr151), and P2 (Olfr17) confirmed the widespread and significant downregulation of OR expression in Mex3a Tg MOEs (Fig. 1g,h). The few remaining OR-expressing neurons in Mex3a Tg MOEs have significantly lower OR IF signal than control MOEs, possibly because they only recently turned on transgenic Mex3a expression under the mOSN-specific tTA driver (Extended Data Fig 1c). Consistent with this, activation of Mex3a expression earlier in OSN differentiation, with two developmentally overlapping tTA drivers, Gg8-tTA¹ and OMP-tTA, induces even stronger effects on OR transcription, with 72% of OR genes significantly

downregulated, and near complete loss of OR immunoreactivity (Fig. 1h, Extended Data Fig. 1d,e,f). Intriguingly, comparison of the effects of ectopic Mex3a expression on OR mRNA vs OR intron sequences shows significantly stronger downregulation of OR mRNAs than their intronic sequences (Fig. 1i). This is consistent with the differentiation-dependent changes in intron/exon ratio of wild type mice (Extended Data Fig. 1a), and supports a post-transcriptional mechanism for OR mRNA silencing in the cytoplasm of Mex3a-expressing mOSNs, likely with a secondary transcriptional downregulation caused by depletion of the OR mRNA¹⁷ and protein³.

To obtain molecular insight into the mechanisms of Mex3a-induced OR silencing, we performed immuno-purification followed by mass spectrometry (IP-MS), using lysates from the MOE (Fig. 2a). Mex3a is technically challenging to IP³², so we compared replicates from multiple experimental conditions to determine high confidence interactors (Fig. 2b). We generated an additional Mex3a Tg line, discussed in detail below, with a mutant RING domain and V5 tag³⁶ to facilitate IP (Extended Data Fig. 2a,b). For each experiment we used a Mex3a-specific or V5-specific antibody and an IgG control, and quantified peptide enrichment in each IP (Fig. 2b, Extended Data Fig. 2b). To exclude proteins that cross-react with the Mex3a antibody, we generated a conditional Mex3a knockout (Mex3a cKO) (Fig. 2c) (Foxg1iresCre³⁷; Mex3a fl/fl³⁸). Mex3a immunoreactivity was abolished from Mex3a cKO MOEs (Fig. 2d), as was detection of a protein band with the expected Mex3a size in western blot from MOE lysates (Fig. 2e). For each genotype, we searched for peptides with a Log₂ fold change of 0.5 or greater enrichment in the Mex3a or V5 IP compared to the respective IgG IP. Putative interacting proteins also exhibited Log₂ fold change of 0.5 or greater enrichment than the Mex3a IP in Mex3a cKO MOE and had a Wilcox p value of less than 0.05 (Fig. 2f, Extended Data Fig. 2c). This analysis uncovered numerous RNA binding proteins with known roles in post-transcriptional silencing (Ago2, Tnrc6b), mRNA degradation (Cnot1, Upf1, Edc4), regulation of mRNA translation (Pum1 and 2, Cpeb4, Fmr1, Fxr2, Pabpc4), as well as numerous ribosomal proteins (Rpl and Rps family members). This interactome is consistent with the hypothesis that Mex3a is involved in post-transcriptional OR silencing affecting both OR mRNA stability and OR mRNA translation, explaining why ectopic Mex3a expression has a stronger effect on exonic OR sequences.

To further distinguish between transcriptional and post-transcriptional Mex3a-dependent OR silencing, we devised a genetic strategy that would uncouple the two processes. Specifically, we crossed our Mex3a Tg mice to mice that express the transgenic OR M71, also under the control of the tetO promoter (tetO-M71iresLacZ³⁹, referred as M71 Tg). In this scheme both transgenes have a tetO promoter and, therefore, are activated by the same transcription factor (tTA) (Fig. 3a). If OR downregulation is induced by transcriptional OR silencing, the transgenic M71 should not be affected, resulting in frequent co-expression with Mex3a. On the other hand, if OR downregulation is post-transcriptional, Mex3a should silence the co-transcribed M71 Tg. Consistent with the latter, M71 Tg expression frequency is dramatically reduced in the presence of the Mex3a Tg (Fig. 3b, e, Extended Data Fig. 3a). Furthermore, the rare mOSNs that still express M71 protein in the double transgenics express greatly reduced levels of the Mex3a Tg (Fig. 3i). Moreover, RNA FISH shows that M71 mRNA detection is also strongly reduced in Mex3a-expressing MOEs (Extended Data Fig. 3b). Mex3a suppresses the expression of another tetO-induced OR, the P2iresGFP knock-in allele^{17,40} when induced by OMP-tTA, or with both Gg8-tTA and OMP-tTA (Fig. 3c,d,e, Extended Data Fig. 3c,d). In contrast, we detect abundant co-expression between Mex3a and the tetO-driven GFP Tg that does not contain OR sequences (Fig. 3f,g, Extended Data Fig. 3e),

excluding the possibility for competition between transgenes for tTA recruitment as an explanation of the mutually exclusive expression pattern. Finally, it is worth noting that when we induce M71 or P2 by both Gg8-tTA and OMP-tTA, we observe reduced coexpression with endogenous Mex3a protein, which is still expressed in Gg8⁺ cells. In contrast, endogenous Mex3a has significantly more frequent co-expression with the GFP Tg (Extended Data Fig. 3g,h), further supporting Mex3a selectivity for OR sequences. Thus, in a striking concurrence between transcriptomics, proteomics, and genetics, our data suggest that endogenous and ectopic Mex3a silence OR gene expression post-transcriptionally.

To obtain deeper mechanistic understanding of Mex3a-mediated OR silencing, we modified the only known enzymatic domain of this protein, the RING domain, which has E3 ubiquitin ligase activity³³. Four distinct point mutations were introduced to the tetO-Mex3a-t2A-mCherry transgene, which disrupt the RING domain's cross-brace structure required for its interaction with zinc⁴¹. Driving this mutant Mex3a transgene (Extended Data Fig. 2a,b) (referred to as Mex3a_{mut} Tg) together with the M71 Tg in mOSNs resulted in abundant expression of M71 and frequent co-expression of the M71 and mutant MEX3A proteins in the same cell (Fig. 3h,i and Extended Data Fig. 3f), in striking contrast to the expression pattern for M71 with the WT Mex3a Tg (Fig. 3b). In addition, FACS isolation followed by RNA-seq of mOSNs expressing the Mex3a_{mut} Tg confirms a significantly reduced ability to silence OR expression genome-wide compared to the WT Mex3a Tg (Fig. 3j). Thus, Mex3a does not simply act as a scaffold protein that recruits known post-transcriptional repressors, but actively contributes to OR silencing via its enzymatic E3 ubiquitin ligase activity. Importantly, IP-MS with the Mex3a_{mut} Tg, does not reveal significant alterations in the interactions between Mex3a and other RNA-binding proteins (Extended Data Fig. 2c), excluding the possibility that RING mutations altered the Mex3a interactome. We cannot exclude however, the intriguing possibility that these presumed Mex3a co-factors silence OR mRNAs in a ubiquitination-dependent fashion.

Mex3a deletion enables OR protein expression in earlier differentiation stages

Our analyses thus far have demonstrated that ectopic Mex3a expression in mOSNs induces post-transcriptional OR silencing that depends on a functional RING domain and likely occurs in coordination with a complex milieu of other post-transcriptional repressors. However, these results do not provide insight to the physiological role of Mex3a in the OSN progenitors that express the endogenous Mex3a protein. A direct expectation from our observations in the gain of function experiments is that loss of Mex3a activity will result in an increase of OR mRNA and protein in OSN progenitors, when Mex3a is expressed.

To test the effects of Mex3a deletion on OR expression, we turned our attention to the Mex3a cKO mice that we described in the IP-MS section (Fig. 2c,d,e). We first performed scRNA-seq in control and Mex3a cKO MOEs (Fig. 4a and Extended Data Fig. 4a,b), with the goal of quantifying changes in OR mRNA abundance across differentiation. Overall, control and Mex3a cKO MOEs have almost identical cell type composition (Extended Data Fig. 4c), suggesting that Mex3a deletion does not cause gross differentiation defects. However, consistent with the hypothesis that Mex3a represses OR expression during the polygenic state of OR transcription, we detect a significant increase in the number of cells expressing multiple ORs (Extended Data Fig. 4d), and the number of OR genes co-transcribed in Mex3a cKO INPs (Fig. 4b, Extended Data Fig. S4E). In addition, we find a significant increase in the number of total OR mRNAs detected in INPs and

iOSNs (Fig. 4c). These differences dissipate in mOSNs, consistent with a developmentally transient Mex3a role on OR mRNA stability that does not extend to the singular phase of OR transcription.

Because Mex3a interacts with proteins with a known function in translational regulation (Fig. 2f), it is possible that it promotes both OR mRNA degradation and repression of OR mRNA translation. To explore whether Mex3a has this dual function in OR gene regulation, we performed ribosome profiling⁴² in OSN progenitors and mOSNs from control and Mex3a cKO mice (Fig. 4d,e,f, Extended Data Fig. 4f,g). To isolate OSN progenitors, we crossed the Mex3a cKO to Ngn1-GFP Tg mice, while to isolate mOSNs we crossed-in the OMP-GFP knock-in allele. Ribosome profiling of sorted Ngn1-GFP⁺ cells revealed increased OR mRNA translation upon deletion of Mex3a (Fig. 4e,f), as measured by ribo-seq counts in the CDS relative to mRNA-seq counts in the same CDS^{42,43}. The increase of translational efficiency observed for OR mRNAs in the Mex3a cKO Ngn1-GFP⁺ cells is not generalized, as a whole, to the rest of the transcriptome (Fig. 4e,f). Moreover, similar analysis in FAC-sorted, OMP-GFP⁺ mOSNs, did not reveal differences in OR translational efficiency between control and Mex3a cKO (Extended Data Fig. 4f,g), further supporting a transient role for Mex3a in suppressing OR mRNA translation only during polygenic OR transcription. Thus, while Mex3a destabilizes the OR mRNA, it also inhibits the translation of the OR mRNAs that were not degraded, consistent with the role of the first Mex3 protein isolated in *C. elegans*⁴⁴.

To independently confirm the observation that OR protein synthesis is developmentally accelerated in Mex3a cKO mice, we performed IF using a pool of antibodies against the ORs P2 (Olfr17), C6 (Olfr49), and M71 (Olfr151) on MOE sections from control and Mex3a cKO Ngn1-GFP mice (Fig. 4g). GFP intensity is highest at the late INP/ early iOSN stage and diminishes with further differentiation. Thus, if OR protein expression occurs at earlier differentiation stages, we should detect increased GFP fluorescence in cells immunoreactive for these OR antibodies. Indeed, as suggested by our ribosome profiling data, Ngn1-GFP intensity is significantly increased in OR⁺ cells from the Mex3a cKO MOEs. Moreover, OR⁺ cells are detected closer to the basal layer of the MOEs of Mex3a cKO mice, confirming that these are OSN progenitors that initiated OR protein expression earlier in development (Fig. 4h,i).

Having established that Mex3a post-transcriptionally represses ORs in OSN progenitor cells, we explored the biological significance of this regulatory mechanism. We reasoned that heterochronic OR translation could increase Perk signaling levels before the onset of singular OR transcription. To test this, we performed IF for Unfolded Protein Response (UPR)-induced transcription factor Atf5, which represents a *bona fide* marker for Perk signaling in OSNs³. Quantification of Atf5 immunoreactivity in MOE sections revealed a significant increase in Atf5 protein expression in Mex3a cKO mice, compared to control littermates (Fig. 5a,b). To further explore UPR and Perk signaling, we generated two lists of genes and computed their module scores⁴⁵ in cells from our scRNA-seq experiment. We identified 318 genes from bulk RNA-seq experiments of sorted cells whose expression peaks in Atf5 translating cells (Extended Data Fig. 5a,b). Computing the module score for these genes, termed “Atf5 translating score,” demonstrates a high score in iOSNs, as expected. To determine if Mex3a cKO results in earlier UPR signaling, we compared the Atf5 translating scores of WT and Mex3a cKO INP cells, before UPR and Perk signaling should occur. We detect a significant increase in the Atf5 translating scores of Mex3a cKO INP cells (Fig. 5c),

supporting the hypothesis that early OR translation induces early UPR signaling. To explore UPR signaling strength further, we used a list of 272 genes that exhibit Atf5 ChIP-seq peaks near their promoters and are differentially expressed in iOSNs of Atf5 KO scRNA-Seq (Kahiapo 2020), termed “Atf5 dependent genes.” We observe significant increase in expression of this class of genes across OSN differentiation (Fig. 5d,e) Taken together, conditional Mex3a deletion from the MOE causes increased OR mRNA detection, OR mRNA translation, and OR protein detection, resulting in stronger Perk signaling induction at a stage that precedes singular OR transcription.

Mex3a deletion biases OR gene choice and disrupts axon guidance specificity.

The realization that Mex3a deletion accelerates OR protein expression and Perk induction raises questions about the functional consequences of these heterochronic changes. Our scRNA-seq data suggest that Mex3a cKO OSNs transition to singular OR transcription with the same efficiency as control OSNs (Fig. 4c, Extended Data Fig. 4d,e). This is not surprising given what we know about the OR-elicited feedback and the process that promotes transition to singular OR transcription. The OR elicited feedback shuts off expression of lysine demethylase Lsd1, preventing both the activation of additional OR alleles (via H3K9 demethylation) and the silencing of the already chosen OR (via H3K4 demethylation)²¹. In contrast, our recent work suggests that transition from polygenic to singular OR transcription is mediated by the non-coding functions of the nascent OR mRNA, and singular OR transcription precedes the OR-protein elicited feedback signal¹⁷. Thus, while loss of the OR-elicited feedback results in unstable OR gene choice, premature induction of this feedback in INPs or early iOSNs does not interfere with the stability and singularity of OR transcription in mOSNs. Then, what is the biological significance of delaying mRNA OR translation and Perk induction until a single OR is chosen?

We recently showed that OR genes are transcriptionally activated at different stages of OSN differentiation, with ORs expressed in ventral MOE regions (zones 4 and 5) detected in more differentiated cells than ORs with dorsal identities (zones 1-3)²⁰. We therefore asked if premature induction of the OR-elicited feedback signal in Mex3a cKO mice disadvantages late onset ORs. Indeed, scRNA-seq experiments from micro-dissected ventral MOE zones show that in Mex3a cKO MOEs, ventral ORs are less likely to be activated during differentiation (Fig. 6a). Moreover, bulk RNA-seq of FAC-sorted mOSNs from the whole MOE showed reduced frequency of choice of ventral, zone 5 (and less so of zone 4) OR genes (Fig. 6b). Thus, premature induction of Perk signaling may narrow the developmental window of OR transcriptional activation, making the transcription and future choice of “delayed” OR genes less likely.

Beyond assuring that the whole OR repertoire can participate in the competitive process of OR gene choice, the precise developmental timing of OR protein expression and Perk induction likely contributes to axon guidance precision. Indeed, Ddit3, the Perk-induced transcription factor that transforms OR protein identity into distinct axon guidance signatures, exhibits significantly increased transcription in Mex3a cKO immature OSNs (Fig. 6c). This prompted us to analyze axonal projections in Mex3a cKO mice. We bred four OR-IRES-GFP lines (OR: Mor23, Mor28, M71, or P2) into the Mex3a cKO mice (Mex3a fl/fl; Foxg1iresCre; OR-IRES-GFP) and explored the effects of Mex3a deletion on glomerular targeting. For all four of these ORs, we observed a significant increase in abnormal axonal wiring to OR-specific stereotyped glomeruli, including missing glomeruli, mispositioned glomeruli, glomeruli with axons extending to other glomeruli of the same OR, and ectopic/micro-glomeruli (Fig. 6d,e,f and Extended Data Fig. 6). Thus,

conditional Mex3a deletion not only results in UPR and Ddit3 dysregulation but also in disruption of the peripheral olfactory circuit, highlighting the importance of post-transcriptional OR gene regulation for the proper development and function of the peripheral olfactory circuit.

Discussion

Our experiments assign Mex3a as a post-transcriptional repressor of OR gene expression during mOSN differentiation. Mex3a expression is exquisitely restricted to INP and iOSN stages, when singular OR choice occurs, and when multiple ORs are expressed per cell. Our gain of function experiments demonstrate robust repression of OR RNA and protein, even when OR expression is driven with a tetO promoter. Loss of function experiments reveal increased OR mRNA per cell, increased OR translational efficiency, and early and more robust Perk signaling.

Neither RNA IP experiments nor HyperTRIBE experiments revealed OR mRNA bound to Mex3a (data not shown). Our experiments with the tetO-M71 Tg do suggest, however that the OR CDS is sufficient for post-transcriptional silencing by Mex3a. This result invites the exciting possibility that Mex3a does not target ORs by binding them directly but selectively represses them via a conserved layer of gene regulation that closely regulates OR translation. Our data invoke several hypotheses for this mechanism of action. Our proteomics analysis proposes that Mex3a recruits proteins with known functions in post-transcriptional gene silencing and mRNA destabilization to the OR mRNA. Moreover, interactions with inhibitors of mRNA translation and with ribosomal proteins suggest that Mex3a may also target OR mRNAs as they engage in translation, explaining why Mex3a deletion results in increased translational efficiency of ORs. Furthermore, the requirement for an intact RING domain for efficient OR silencing by Mex3a proposes three possible scenarios for the role of lysine ubiquitination: First, the activity of some of the Mex3a interacting proteins that contribute to post-transcriptional silencing may be increased by ubiquitination. Second, ubiquitination may cause proteosomal degradation of some of the critical ribosomal proteins engaged in OR mRNA translation. Third, Mex3a may also ubiquitinate the OR polypeptides as they are translated by the ribosome, resulting in immediate post-translational degradation by the proteasome.

In Mex3a cKO animals, we observe increased Atf5 nuclear staining as well as increased transcription of Atf5 downstream targets. Increased OR translation in Mex3a cKO MOE may suffice to elicit the Unfolded Protein Response, explaining these findings. An alternative possibility is that instead of directly targeting OR mRNA stability or translation, Mex3a acts to repress UPR signaling which in turn prevents OR translation before singular OR choice has been established. If Mex3a functions by modulating UPR signaling, then other GPCRs or ER-translated proteins may also be targets of Mex3a regulation. Mex3a is expressed in stem cell niches of multiple tissues including the intestinal crypt²⁹, and prenatal cerebral cortex⁴⁶, whose differentiated cell types express high levels of transmembrane bound receptors. Reports also demonstrate that the UPR signaling pathway is an integral part of cellular differentiation in these systems^{47,48}. Our findings in the olfactory epithelium invite the exciting hypothesis that Mex3a may repress transmembrane bound proteins in immature cells of other tissues before they undergo differentiation.

The intricate network of post-transcriptional OR regulation that we report here raises an important question: If OSNs have a mechanism in place that assures absolute transcriptional singularity, why not use it from the very beginning, surpassing any need for post-transcriptional repression? Recent

observations from single cell genomic analyses suggest that the nucleoprotein apparatus that assures robust OR transcription, the multi-chromosomal enhancer hub, requires OR transcription for its assembly over any OR allele or for its recruitment to an OR locus. However, because OR promoters have extensive homology with each other⁴⁹, OSN progenitors cannot activate only a single OR at once. Instead, they deploy polygenic transcription to generate nuclear architecture landscapes that are conducive to singular OR transcription through enhancer hub competition¹⁸ and an RNA-mediated symmetry breaking process¹⁷. Thus, if the differentiating OSNs had to use the identity of the expressed OR protein as a trigger for the feedback signal and a compass for axon targeting, they would need to deploy a transient post-transcriptional mechanism operating outside of the nucleus to uncouple the obligatory polygenic OR transcription from OR translation until singularity is established. It appears that Mex3a, with a strictly cytoplasmic distribution in the MOE, plays this critical function in the olfactory system.

Our Mex3a loss of function experiments reveal what the consequences would be for the developing olfactory system if polygenic OR transcription resulted in more efficient OR protein expression. Specifically, our observations from the Mex3a cKO mice suggest that post-transcriptional OR silencing during polygenic OR transcription has three important functions for olfaction: it prevents premature induction of the OR-elicited feedback signal, ensures that the entire repertoire of ORs has the opportunity to be chosen, and insulates OR-directed axon guidance from the conflicting signals of the co-transcribed ORs. When this insulation is perturbed by Mex3a deletion, the onset of OR translation is developmentally accelerated, and the levels of Perk signaling increase before the transition to singular OR transcription, resulting in biased OR gene choice and OSN axon mistargeting. ORs from ventral zones, which are less likely to be expressed in Mex3a cKO mice, require additional layers of heterochromatin and nuclear organization to be chosen²⁰. These processes may mean that zone 4 and 5 ORs need more developmental time to be selected. Our observation that dorsal zone 1-3 ORs are chosen at a higher frequency in Mex3a cKO animals is likely caused by precocious Perk signaling, which spurs iOSNs to differentiate before enough time has elapsed to ensure ventral zone 4 and 5 OR choice. Indeed, previous work demonstrates that modulating Atf5 translation, which is a direct target of Perk signaling, in the MOE can influence receptor choice in OSNs³. Zonal organization of ORs facilitates axonal wiring to the bulb. Mex3a deletion results in striking axon guidance defects, where stereotyped positions of glomeruli are shifted dramatically, and axons form microglomeruli or extend to sister glomeruli expressing the same OR. Previous work in our lab uncovered the direct link between Perk signaling strength and axon guidance precision to OR specific glomeruli⁷. Our work supports this finding and suggests that precocious Perk signaling and biases in OR choice have profound effects on axon guidance and the olfactory bulb map. It should also be noted that the biological significance of post-transcriptional OR silencing may be underestimated by the conditional Mex3a deletion, as the close paralogues Mex3b and Mex3c are still expressed, albeit at lower levels, and may provide redundant functions in INPs and iOSNs.

In summary, we have uncovered a novel regulatory function for Mex3a, a protein studied almost exclusively in the context of stem cell maintenance and renewal in physiological contexts^{30,31}, and as a pro-proliferative, oncogenic factor in tumors^{33,38}. Persistent Mex3a expression in post-mitotic cells of the MOE, and post-transcriptional silencing of the largest mammalian gene family, suggest that this protein and its paralogues may have additional functions that extend beyond the regulation of cell cycle and cell signaling pathways controlling cell division rates. In fact, our data suggest

that Mex3a plays a crucial role in influencing the identity and eventual connectivity of post-mitotic OSN progenitors, a conceptually similar function with the *C. elegans* homologue, which specified anterior-posterior asymmetry and the fate of blastomere descendants⁴⁴. If the OR CDS constitutes a generalizable target for post-transcriptional silencing, many of our observations are likely applicable to other GPCRs with extensive homology to the OR superfamily. In future studies, it will be interesting to explore whether Mex3a post-transcriptionally represses GPCRs or other ER translated proteins in the diverse repertoire of tissues and cancer cell types where it is expressed.

Figure Legends

Fig. 1: Mex3a silences OR expression in olfactory neurons

a, OR mRNA levels quantified across three stages of the olfactory neuronal lineage by single cell RNA-Seq (left panel) and single nucleus RNA-Seq (right panel). Statistics calculated using Wilcoxon rank sum test. **b**, Mex3 family members *Mex3a*, *Mex3b*, *Mex3c*, and *Mex3d* expression patterns by bulk RNA-Seq of two replicates each of FAC sorted cells (details in extended methods) over olfactory neuronal differentiation. Error bars, standard error. **c**, Representative immunofluorescence image from greater than 10 biological replicates in wildtype, four-week-old olfactory epithelium, staining for Mex3a (green) and neuronal marker Vglut2 (magenta), DAPI in blue. Scalebar 30 μ M. **d**, Diagram of Mex3a Tg allele (left panel). Elements of the construct labeled on the figure. Right, Immunofluorescence image in OMP-tTA; Mex3a Tg olfactory epithelium, staining for Mex3a (green) and mCherry (magenta), DAPI in blue. Scalebar 30 μ M. **e**, MA plot of differentially expressed genes from bulk RNA-Seq comparing OMP-tTA; Mex3a Tg to OMP-tTA; GFP Tg. Significant ORs shown in red, significant non-OR mRNAs shown in blue. Statistics calculated with DESeq2, $p_{adj} < 0.05$, \log_2 fold change threshold, 0.5849. **f**, Violin plot quantifying all OR mRNAs and non-OR mRNAs in bulk RNA-Seq from OMP-tTA; Mex3a Tg compared to OMP-tTA; GFP Tg. Statistics calculated with Welch two sample t-test. **g**, Immunofluorescence image in OMP-tTA; Mex3a Tg (right) and littermate control (left), staining for OR proteins C2, M71, Mor28, and P2. ORs shown in white, background fluorescence delineates contours of olfactory tissue. Scalebar 100 μ M. **h**, Quantification of number of ORs (Mor28, C6, P2, M71) detected by IF per coronal section of the olfactory epithelium. N=two or more biological replicates per condition. Statistics, Welch two sample t-test. **i**, Violin plot quantifying OR exonic and intronic reads in bulk RNA-Seq from OMP-tTA; Mex3a Tg compared to OMP-tTA; GFP Tg. Statistics calculated using Wilcoxon rank sum test.

Fig. 2: Mex3a protein interactome identifies proteins with known post-transcriptional roles

a, Experimental design for Immunopurification-Mass Spectrometry experiment. Whole MOE was lysed and subjected to IP using a Mex3a or V5 antibody, or IgG antibody as negative control. Immunopurified proteins were sequenced by mass spectrometry. **b**, Resulting peptides compared to IgG controls from the same protein samples across the four genotypes (described in panel above the plots) are shown. Two replicates shown for each genotype except for Mex3a cKO, where four replicates are shown. Mex3a peptides shown in blue. **c**, Diagram of Mex3a cKO allele. CDS is

shown with thicker gray rectangle, and 3'UTR is shown with a thin gray rectangle. KH domains in orange and RING domain in blue. The first KH domain spans an intron (thin gray line). Flox elements excise the CDS in the second exon. **d**, Representative immunofluorescence image from greater than ten biological replicates in Mex3a cKO and littermate control showing loss of Mex3a protein (green) in the MOE when the Mex3a flox allele is excised with a Foxg1iresCre allele. Scalebar 25 μ M. **e**, Western blot of two biological replicates of whole MOE at PN12 for Mex3a (green) and loading control PCNA (magenta). Mex3a predicted at 58kDA, PCNA predicted at 29kDA. **f**, STRING representation of Mex3a interacting proteins, generated with Cytoscape software. After identifying peptides that were enriched 0.5 Log Fold greater than IgG IPs, six replicates (first three panels of Fig. 2b) were compared to peptides enriched in the Mex3a cKO IPs. Peptides passing a threshold of 0.5 log fold higher than Mex3a cKO, and a Wilcoxon rank sum test resulting in a p value of 0.05 or lower, were considered candidates for Mex3a protein interacting partners. Log fold enrichment greater than IgG is represented by the size of the circle, and color represents p value relative to Mex3a cKO. Weight of the lines between proteins is based on STRING prediction of interaction, with thicker lines representing strongest evidence of interaction.

Fig. 3: Post-transcriptional silencing of Olfactory Receptors with the Mex3a Tg

a, Schematic depicting genetic strategy to test post-transcriptional role of Mex3a. Both Mex3a and OR/GFP transgenic alleles are driven by cell-type specific OMP-tTA and/or gg8-tTA alleles in the same nucleus. IF offers a read out of protein abundance in the presence or absence of the Mex3a Tg. **b**, Immunofluorescence for Mex3a (green) and M71 (magenta) in (left) OMP-tTA; M71 Tg (“monoclonal nose”) and (right) OMP-tTA; M71 Tg; Mex3a Tg. **c**, Immunofluorescence for Mex3a (green) and P2 (magenta) in OMP-tTA; P2 Tg on left, and right, OMP-tTA; P2 Tg; Mex3a Tg. **d**, Same as 3C, except both genotypes include the gg8-tTA and OMP-tTA drivers. **e**, Mean OR fluorescence intensity per image. N equals two to four biological replicates per condition, 4-16 images per condition. Statistics calculated with Welch two sample t-test. **f**, Immunofluorescence for Mex3a (green) and GFP (magenta) in gg8-tTA; OMP-tTA; GFP Tg; Mex3a Tg. **g**, Pearson correlations comparing colocalization between Mex3a and P2 fluorescent channels in the gg8-tTA; OMP-tTA; P2 Tg Mex3a Tg and Mex3a and GFP fluorescent channels in the gg8-tTA; OMP-tTA; GFP Tg, Mex3a Tg. Statistics calculated with Welch two sample t-test. **h**, Immunofluorescence for Mex3a (green) and M71 (magenta) in OMP-tTA; M71 Tg; Mex3a_{mut} Tg. Scalebar, 25 μ M (same scale for all images in Fig. 3) **i**, Quantification of M71 positive cells in mice from (A) and (G) that exhibited Mex3a co-expression (yellow), or M71 only (green). Statistics, Fisher’s exact test. **j**, Bulk RNA-Seq from OMP-tTA; Mex3a_{mut} Tg compared to OMP-tTA; Mex3a Tg. Left, MA plot of OR mRNAs. Statistics calculated with DESeq2, padj < 0.05, log₂ fold change threshold, 0.5849. Right, violin plot comparing all OR mRNAs to non-OR mRNAs. Statistics calculated with Welch two sample t-test.

Fig. 4: Ectopic OR expression upon loss of Mex3a.

a, UMAP plot of single cell RNA-Seq data from two replicates of Mex3a cKO and Mex3a WT littermate controls, whole MOE at PN12. Markers found for each cluster were used to infer cell type. **b**, OR mRNA was assessed in single cells from the Immediate Neuronal Progenitor (INP) stage. Cells expressing more than one OR with a threshold of >1 normalized counts were analyzed,

and the number of different OR genes in the same cell is quantified in Mex3a WT and Mex3a cKO INP cells. **c**, OR mRNA levels were assessed in single cells from the neuronal lineage. Any cell with a threshold of >1 normalized count for an OR was included (n for each condition is equal to the number of cells that passed this threshold). Statistics calculated with Wilcoxon rank sum test with continuity correction. **d**, Schematic of the ribosome footprinting technique. Ribosomes in blue, mRNA in red. Translation efficiency is a measure of the riboprofiling-Seq counts in the CDS of a gene relative to the RNA-Seq counts in the same CDS. **e**, Scatter plot comparing Log2 Fold Change Translational Efficiency (y-axis) and Log2 Fold Change RNA transcript per million (x-axis) in two replicates of Mex3a cKO vs Mex3a WT Ngn1-GFP sorted cells, PN12 aged mice. Red dots, OR RNAs, gray dots, non-OR RNAs. Blue line, linear regression line. Marginal density plots summarize OR gene family (red) or all other genes (gray) Translational Efficiency (y-axis) or RNA expression levels (x-axis). **f**, Violin Plot quantifying translational efficiency of OR mRNAs (red) compared to non-OR mRNAs (gray) in two replicates of Mex3a cKO vs Mex3a WT Ngn1-GFP sorted cells. Statistics calculated with Welch two sample t-test. **g**, Representative immunofluorescence image from three biological replicates at four weeks old, Mex3a WT littermate controls and Mex3a cKO. Endogenous Ngn1-GFP labeling is visualized in green, OR protein shown in magenta, DAPI in blue. A pool of M71, P2, and C6 OR antibodies were used. Images from Mex3a WT and cKO are from the same zonal position in the olfactory epithelium. Scalebar, 25 μ M. **h**, Violin plot quantifying Ngn1-GFP fluorescence intensity in each OR positive cell (dots) from the Mex3a WT (left) and cKO (right) immunofluorescence experiment described in G. N is equal to the number of OR positive cells counted for each genotype. Statistics, Wilcoxon rank sum test. **i**, Violin plot quantifying relative position (for each image, the basal position of the OE is set to 0 on the y-axis, apical set to 1) in olfactory epithelium of OR positive cells (dots). N is equal to the number of OR positive cells counted for each genotype. Statistics, Wilcoxon rank sum test.

Fig. 5: UPR-induced transcription factor Atf5 and targets exhibit increased expression in the Mex3a cKO

a, Representative immunofluorescence image from three biological replicates at PN12, Mex3a WT littermate controls and Mex3a cKO. Atf5 staining in green, DAPI in blue. Images from Mex3a WT and cKO are from the same zonal position in the olfactory epithelium. Scalebar, 25 μ M. **b**, Violin plot depicting mean Atf5 signal intensity of Atf5⁺ individual cells, quantified from images taken from all zones of the olfactory epithelium. Each dot is a cell, N is equal to the number of Atf5 positive cells counted for each genotype. **c**, Violin plot quantifying “Atf5 translating” module score from scRNA-Seq data, Immediate neuronal progenitor cells, comparing Mex3a WT and cKO. The Atf5 translating score is calculated from 318 genes whose expression peaks in bulk RNA-Seq sorted cells from an Atf5 iRFP reporter allele compared to Ngn1-GFP and OMP-GFP sorted cells (see S5A and B). Cells with a higher score are more likely to be translating Atf5. **d**, UMAP plot which splits Mex3a WT (left) and Mex3a cKO (right) cells. Cells are colored based on their module score for “Atf5 dependent genes,” which is calculated from 272 genes whose expression changes by scRNA-Seq in Atf5 cKO compared to littermate controls, and which also have an Atf5 ChIP peak close to their promoters. Cells with a higher score have higher transcription of Atf5 “target” genes. **e**, Violin plots quantifying Mex3a WT compared to cKO “Atf5 dependent gene” module scores across the neuronal lineage. N is equal to the number of cells from each genotype in each cell stage. Statistics, Wilcoxon rank sum test.

Fig. 6: Mex3a cKO biases OR gene choice and disrupts axon guidance specificity

a, Barplot quantifying zonal OR expression in scRNA-Seq from micro-dissected MOE from two biological replicates of four-week Mex3a cKO and Mex3a WT littermate controls. Top two panels, scRNA-Seq from dorsal dissection of MOE. Bottom two panels, scRNA-Seq from ventral dissection of MOE. Mex3a cKO is shown as the second panel in each case. Sum of all OR counts in cells from mature OSN clusters only. **b**, Barplot quantifying OR mRNA from three biological replicates of OMP-GFP sorted neurons from Mex3a cKO and Mex3a WT littermate controls. ORs (dots) are divided into known zones. Statistics, ANOVA one-way test. **c**, *Ddit3* mRNA levels measured in single cells (dots) from PN12 scRNA-Seq shown in Fig. 4a, immature and mature OSNs only. Statistics, Wilcoxon rank sum test (Seurat's FindMarkers). **d**, Representative whole mount image from 22 biological replicates of an olfactory bulb from Mex3a WT; Mor28 GFP (ventral view). Mor28 glomeruli and axon fibers shown in white. Lower panels show magnification of lateral glomeruli. **e**, Representative whole mount image from 41 biological replicates of an olfactory bulb from Mex3a cKO; Mor28 GFP (ventral view). Mor28 glomeruli and axon fibers shown in white. Lower panels show magnification of lateral glomeruli. **f**, (Top) Barplot quantifying abnormal phenotypes of individual glomeruli from four different OR-ires-GFP lines mated with Mex3a cKO and WT littermate controls. N equals number of glomeruli. Glomeruli are considered abnormal if they exhibit any of the phenotypes described in G. Statistics, Fisher's Exact test. (Bottom) Stacked barplot depicting proportions of glomeruli from a given OR that exhibit abnormal wiring phenotypes (missing, mispositioned, reaching axons, ectopic or microglomeruli). N equals number of glomeruli. Statistics, Fisher's Exact test. **g**, Model for Mex3a regulation of OR genes during OSN differentiation. Mex3a expression peaks during the INP stage, when multiple OR genes are expressed per cell. Mex3a mediated repression of OR mRNAs/translation in the cytoplasm allows the neuron to undergo changes to nuclear architecture ensuring OR transcriptional singularity without triggering the unfolded protein response. Immature OSNs: As Mex3a expression wanes, OR mRNAs in the cytoplasm cease to be repressed and the unfolded protein response is activated. In mature OSNs, Mex3a is no longer expressed and OR translation increases.

Supplementary Figure Legends

Extended Data Fig. 1: related to Fig. 1

a, Ratios between OR introns and exons for all ORs that are expressed through the neuronal lineage in WT cells isolated by genetic labeling of distinct olfactory sensory neuron cell types (See extended methods, same RNA-Seq dataset as shown in Fig. 1b). **b**, PCA plot of bulk RNA-Seq samples for Mex3a Tg experiments. Two biological replicates per sample. Sorted cells from the MOE using CD54 antibody (Icam) or endogenous labeling (GFP for Ngn1-GFP, OMP-GFP, and GFP Tg; tdTomato for *Ascl1*, mCherry for Mex3a Tg and Mex3a_{mut} Tg). **c**, Violin plot quantifying mean M71 signal per M71+ cell (dots) in IF images from OMP-tTA; M71 Tg vs OMP-tTA; M71 Tg, Mex3a Tg genotypes. N is equal to the number of cells quantified for each genotype. Statistics, Welch two sample t-test. **d**, MA Plot of differentially expressed genes in gg8-tTA; OMP-tTA; Mex3a Tg compared to gg8-tTA; OMP-tTA; GFP Tg. Significant ORs (red dots), Significant non-ORs (blue dots). **e**, Violin Plot quantifying OR mRNA and non-OR mRNA in Mex3a Tg (both

tTA drivers) compared to GFP Tg (both tTA drivers). Statistics, Welch Two Sample t-test. **f**, Representative immunofluorescence image from four biological replicates per genotype, scale bar 100 μ M.

Extended Data Fig. 2: related to Fig. 2

a, Design of the Mex3a_{mut} Tg allele. Four point-mutations in the RING domain render the protein unable to bind the zinc required for ubiquitination activity. A V5 allele was added to facilitate Immunoprecipitation experiments. **b**, Representative Immunofluorescence image from the gg8-tTA; OMP-tTA; Mex3a_{mut} Tg mouse compared to a littermate control. Mex3a in green, Calmegin (ER marker that is expressed in mOSNs) in magenta, DAPI in blue. Scalebar 25 μ M. **c**, Scatterplot showing mean enrichment in Mex3a/V5 Immunoprecipitations from two biological replicates of 1) WT 2) gg8-tTA; OMP-tTA; Mex3a Tg 3) gg8-tTA; OMP-tTA; Mex3a_{mut} Tg. Mean enrichment compared to IgG controls shown on the x-axis, mean enrichment compared to Mex3a immunoprecipitation from Mex3a cKO samples shown on the y-axis. Each dot is a protein, blue labels highlight known post-transcriptional regulators/RNA-binding proteins. Red label highlights Mex3a. Dotted lines show cut-offs used in analysis to generate Fig. 2f.

Extended Data Fig. 3: related to Fig. 3.

a, Grayscale images of M71 and Mex3a channels shown in Fig. 3b. **b**, RNA *In situ* hybridization using a probe for M71 RNA (left, Red, right, grayscale of same image) in OMP-tTA; M71 Tg and OMP-tTA; M71 Tg; Mex3a Tg. Right, boxplot quantifying Mean M71 ISH signal per image. N is equal to 5 images (M71 Tg alone) and 9 images (M71 Tg; Mex3a Tg). Statistics, Welch two sample t-test. **c**, Grayscale images P2 and Mex3a channels shown in Fig. 3c. **d**, Grayscale images P2 and Mex3a channels shown in Fig. 3d. **e**, Grayscale images GFP and Mex3a channels shown in Fig. 3f. **f**, Grayscale images M71 and Mex3a channels shown in Fig. 3h. **g**, Immunofluorescence image of OR/GFP (magenta) and endogenous (non-transgenic) Mex3a (green) for three genotypes 1) gg8-tTA; OMP-tTA; M71 Tg 2) gg8-tTA; OMP-tTA; P2 Tg 3) gg8-tTA; OMP-tTA; GFP Tg. Scalebar 25 μ M, same for all images in this figure. **h**, Pearson correlations measuring colocalization between OR/GFP channels and endogenous Mex3a. Statistics, Welch two sample t-test.

Extended Data Fig. 4: related to Fig. 4

a, UMAP plot of single cell RNA-Seq data from two replicates of Mex3a cKO and Mex3a WT littermate controls, whole MOE at PN12. Known markers are highlighted to show cell types (*Ascl1*, globose basal cell; *Neurod1*, immediate neuronal progenitor; *Crabp1*, immediate neuronal progenitor; *Gap43*, immature olfactory sensory neuron; *Omp*, mature olfactory sensory neuron; *Cyp2a5*, sustentacular) **b**, UMAP projection showing Mex3a expression pattern in single cell RNA-Seq data. **c**, Stacked barplot classifying Mex3a WT and Mex3a cKO single cells in the neuronal lineage as GBC, INP, iOSN, or mOSN cells **d**, Stacked barplot classifying GBC, INP, iOSN, and mOSN single cells by whether they are expressing zero, one, or more than one OR per cell. Threshold of >1 normalized count over an OR to be considered expressed. Statistics, Fisher's Exact Test: testing proportion of cells with multiple ORs per cell comparing Mex3a cKO and Mex3a WT. GBC, p=0.65. INP, p= 6.0e-09. iOSN, p= 3.2e-12. mOSN, p= 1.1e-2 **e**, Quantification of number of ORs detected per cell in cells from the category "multiple OR per cell" from **(d)**

(yellow group). N equals number of cells expressing more than one OR in each category. **f**, Scatter plot comparing Translational Efficiency (y-axis) and RNA transcript per million (x-axis) in two replicates of Mex3a cKO vs Mex3a WT OMP-GFP sorted cells. Red dots, OR RNAs, gray dots, non-OR RNAs. Blue line, linear regression line. Marginal density plots summarize OR gene family (red) or all other genes (gray) Translational Efficiency (y-axis) or RNA expression levels (x-axis). **g**, Violin Plot quantifying translational efficiency of OR mRNAs (red) compared to non-OR mRNAs (gray) in two replicates of Mex3a cKO vs Mex3a WT OMP-GFP sorted cells. Statistics calculated with Welch two sample t-test.

Extended Data Fig. 5: related to Fig. 5

a, Line graph showing three examples of genes whose expression peaks in Atf5 translating cells. DESeq2 was used to identify 318 genes that follow this expression pattern and were used in the “Atf5 translating” module score analysis shown in Fig. 5c. **b**, UMAP projection of Atf5 translating scores in Mex3a cKO and WT littermate controls. Higher score means the cell is more likely to be actively translating Atf5. As expected, “Atf5 translating” score peaks in the immature OSN stage.

Extended Data Fig. 6: related to Fig. 6

a, Representative whole mount images of olfactory bulbs from Mex3a WT (top panel) and Mex3a cKO mice (bottom panel). View of the olfactory bulb is labeled, as OR glomeruli have distinct stereotyped positions. Mor23 Mex3a WT (35 mice), Mex3a cKO (12 mice). Mor28 Mex3a WT (22 mice), Mex3a cKO (41 mice). M71 Mex3a WT (32 mice), Mex3a cKO (27 mice). P2 Mex3a WT (34 mice), Mex3a cKO (17 mice).

Materials and Methods

Mice

Mouse protocols were approved by the Columbia University IACUC under protocol numbers AC-AAAT2450 and AC-AABG6553. All mice were housed in standard conditions with a 12-hour light/dark cycle and access to food and water *ad libitum*. Strains used are indicated in Supplemental Mouse Line table. All animals were on a mixed genetic background and littermate controls were used for comparisons. Animals were sacrificed by decapitation (if younger than postnatal day 14) or CO₂ followed by cervical dislocation, and the main olfactory epithelium (MOE) or olfactory bulb was isolated by dissection.

Transgenic Mice were generated with the Genetically Modified Mouse Model Shared Resource at Columbia University. They were constructed with the following plasmids, available on Addgene (IDs 223244 and 223245) tetO-CMV-Mex3a-t2a-mCherry and tetO-CMV-Mex3amutRING-V5-t2a-mCherry. In Fusion cloning (Takara) was used to clone Mex3a that was partially amplified from MOE cDNA, and partially supplied via gene block. The amino acid sequence of *Mus musculus* Mex3a is preserved, however the CG content of the DNA sequence was reduced to facilitate cloning. For the mutant RING transgene, four point-mutations were introduced: Cys 484 Ala; His 486 Ala; Cys 490 Ala; Cys 493 Ala using a gene block (IDT).

Immunofluorescence

Olfactory Epithelium was dissected and placed in O.C.T. compound (Fisher Scientific) for 20 minutes before freezing in a dry ice, ethanol bath. If endogenous genetic labeling was visualized (Fig. 1d, 3f, 4g, Extended Data Fig. 3e,g), olfactory epithelium was prefixed in 4% PFA (Fisher Scientific), 1X PBS for 8 minutes on ice, washed 3X with PBS 1X, and incubated in 30% sucrose, PBS 1X overnight at 4C on a rocking platform, then incubated in O.C.T. compound for 20 minutes before freezing in a dry ice, ethanol bath. Tissue sections were collected at 12um thickness on a Leica cm1950 Cryostat, with control and experimental tissue sections on the same slide to ensure the same experimental conditions throughout. Slides were allowed to come to RT for 10 minutes before fixing in 4% PFA, PBS 1X at RT for 5 minutes in a slide mailer. Slides were washed 3X in PBS 1X, then blocked for one hour in IF blocking buffer: PBS 1X, 4% sterile Donkey Serum (Sigma Aldrich), 1% Triton X-100. Slides were assembled in a humid chamber, and 100uL of blocking plus primary antibody (1:200 dilution) solution was added to the slide. A coverslip was placed over slide and incubated overnight at 4C in the humid chamber. The following day, slides were washed in a slide mailer 3x5 minutes in PBS 1X, Triton 0.1%, then incubated in secondary antibody solution (Jackson Immunoresearch) for 45 minutes at RT. Secondary antibody solution was IF blocking buffer with secondary antibodies diluted 1:500, and 1mg/mL DAPI diluted 1:1000. 100uL of secondary solution was applied to the slide and a coverslip was placed on top. Incubations were conducted in the humid chamber. Slides were washed in a slide mailer for 3x5 minutes in PBS 1X, Triton 0.1%, then mounted with Vectashield antifade mounting medium (Vector Laboratories).

Antibodies: Mex3a (abcam 79046), Vglut2 (Millipore Sigma AB2251-I), OR antibodies (Olf1507, C2, P2, M71) generous gifts from G Barnea (Brown University), Calmegin (Santa Cruz sc-49899), Atf5 (Santa Cruz sc-46934).

Image Acquisition and Analysis

Microscopy: Images were taken on a Zeiss LSM 700 Confocal or a W1-Yokogawa spinning disk Confocal and analysis and quantification were performed using FIJI and NIS-Elements software, with detailed coding found in supplemental Coding file.

Fluorescence activated cell sorting

The olfactory epithelium was dissected into ice cold PBS 1X and cells were dissociated with the Worthington Papain Dissociation System (Worthington Biochemical) according to manufacturer's instructions. Cells were resuspended in PBS 1X supplemented with 10% Fetal Bovine Serum and DNaseI provided with Worthington kit. DAPI was added to exclude dead cells during sorting. Cells were filtered and sorted with either a Beckman Coulter MoFlo Astrios EQ Cell Sorter or a BD Influx Cell Sorter. Sorted cells were centrifuged at 500g with a swinging bucket rotor, and the supernatant was removed. Cells used for RNA-Seq were resuspended in 500uL of TRIzol Reagent (Invitrogen). For Ribosome profiling experiments, all solutions beginning with dissection were supplemented with 100ug/mL Cycloheximide (Sigma Aldrich). After sorting, cell pellets were snap frozen in liquid nitrogen and stored at -80C until processed.

RNA-Sequencing

RNA was extracted from FAC sorted cells using TRIzol reagent (Invitrogen). 1-Bromo-3-chloropropane (Sigma Aldrich) was added to isolate RNA into the upper aqueous phase, and Isopropanol was used to precipitate RNA. GenElute LPA (Sigma Aldrich) was added to facilitate precipitation. The RNA pellet was washed with 75% Ethanol, the pellet was allowed to dry 5 minutes at RT, and resuspended in H₂O. RNA was immediately treated with DNase I (Ambion) at 37C for 30 minutes, and purified using AMPure XP beads (Beckman Coulter). RNA-Seq libraries were made using the SMARTer Stranded Total RNA-Seq Kit - Pico Input (Takara) or TruSeq® Stranded Total RNA Library Prep (Illumina) according to manufacturer's instructions. Comparisons between samples are from the same library preparation kit. Libraries were sequenced on a NextSeq 550 Illumina sequencer. Data were analyzed with DESeq2, with detailed code found in supplemental file. GEO accession [GSE271029](https://www.ncbi.nlm.nih.gov/geo/query/acc.cgi?acc=GSE271029).

Immunopurification Mass Spectrometry (see extended methods for details)

Olfactory epithelium was dissected and lysed in IP lysis buffer (150 mM NaCl, 50mM Tris pH 7.5, 1% NP-40 Igepal Ca-630, 5% glycerol, protease and phosphatase inhibitors) for 30-60 minutes rotating at 4C. Lysates were centrifuged to remove insoluble material, and protein concentration was estimated with the Pierce BCA protein Assay kit (Thermo Fisher Scientific). 1mg of protein was used per IP except for WT mice for the Mex3a/IgG pulldowns where 4mg of protein were used. 10 µg of antibody (Mex3a abcam 79046, V5 abcam 9116, IgG abcam 46540) were added to lysates (volume brought up to 500uL with lysis buffer), and 100 µL of Protein G Dynabeads beads were added per IP. IPs were rotated overnight at 4C. Immunopurified material was eluted, reduced, alkylated, Trypsin digested, and acidified. Peptides were subjected to C18 cleanup, TMT labeling and multiplexing, and LC-MS/MS on a benchtop Orbitrap Q Exactive HF mass spectrometer. See extended methods for additional details pertaining to this experiment. Raw data were analyzed using MaxQuant software and with code found in supplementary Code file. Data are available on the [UCSD Massive repository](https://massive.ucsd.edu/ProteoSAFe/dataset.jsp?task=8db1dde776b0457a9cdb831d1f54fac1) <https://massive.ucsd.edu/ProteoSAFe/dataset.jsp?task=8db1dde776b0457a9cdb831d1f54fac1>.

Western

Olfactory epithelium was dissected and minced in a glass dissection dish on ice. Tissue was lysed at 4C, rotating for 30 minutes in Radio immunoprecipitation assay buffer (RIPA) (the following chemicals from Sigma Aldrich): 150 mM sodium chloride, 1.0% NP-40 Igepal ca-630, 0.5% sodium deoxycholate, 0.1% SDS (sodium dodecyl sulphate), 50 mM Tris, pH 8.0, supplemented with protease inhibitors (Halt Protease inhibitor cocktail, EDTA free, Thermo Fisher Scientific). Lysates were centrifuged to remove insoluble materials, and sonicated using a Covaris Sonicator to sonicate genomic DNA with the settings Duty cycle, 2%; Intensity, 3; Cycles/Burst, 200; Frequency sweeping; Max temp = 6C. Sonicated lysates were quantified using a Pierce BCA protein Assay kit (Thermo Fisher Scientific), and combined with Laemmli 4X loading buffer supplemented with β-Mercaptoethanol. Lysates were loaded onto a 4–20% precast polyacrylamide gel (BioRad) and protein electrophoresis was completed with constant mA. Proteins were transferred to a PVDF membrane, blocked in Intercept (PBS) Blocking Buffer (Licor), and incubated with primary antibodies (Mex3a abcam 79046, 1:3000 dilution, PCNA abcam 139696, 1:3000 dilution) overnight in blocking buffer supplemented with 0.2% Tween-20. The following day, membranes were washed 3x7 minutes in PBS 1X; Tween-20 0.1% and incubated for 1 hour at RT with IRDye secondary antibodies (Licor) in Intercept PBS blocking buffer supplemented

with Tween-20 0.2% and SDS 0.01%. Membranes were washed 3x7 minutes with PBS 1X; Tween-20 0.1%, and imaged on a Licor Odyssey Imaging System.

Ribosome Profiling (see extended methods for details)

Two replicates of Ngn-GFP⁺ and OMP-GFP⁺ cells were collected from olfactory epithelium by FACs from Mex3a WT and Mex3a cKO littermates. Ribosome profiling was performed according to McGlincy and Ignolia 2017, with modifications and details described in extended methods. Code used for analysis can be found in Supplemental Code file. GEO accession [GSE271027](#) for ribosome profiling libraries and [GSE271029](#) for sample matched RNA-Seq libraries.

Single Cell RNA-Sequencing

Olfactory epithelium was dissected and dissociated into single cells using the Worthington Papain dissociation system (Worthington Biochemical). Cells were counted and processed according to manufacturer's instructions using 10X Genomics equipment and reagents from the Chromium Single Cell Gene Expression v3 kit with the help of the Columbia Genome Center. Libraries were sequenced on an Illumina NextSeq 550 Sequencing machine, libraries were aligned with Cell Ranger (10X genomics) with introns included. Data were analyzed using Seurat. Code used for analysis can be found in Supplemental Code file. GEO accession [GSE271031](#)

Glomerulus Analysis

Mice carrying OR-ires-GFP alleles (Mor23iresGFP, Mor28iresGFP, M71iresGFP, P2iresGFP) were bred into the Mex3a flox; Foxg1iresCre line. Mice were allowed to age and sacrificed between 3 and 10 months of age, averaging 5 months old at time of experiment. Olfactory bulbs (OBs) were dissected with a portion of the rest of the brain, carefully separating bulbs from the olfactory epithelium. OBs were kept in PBS 1X on ice until imaged the same day. Bulbs were imaged on a Nikon SMZ18 Stereo Microscope. Once whole OB images were taken, OB lobes were hemisected to reveal and image additional glomeruli.

Bibliography

1. Nguyen, M.Q., Zhou, Z., Marks, C.A., Ryba, N.J., and Belluscio, L. (2007). Prominent roles for odorant receptor coding sequences in allelic exclusion. *Cell* 131, 1009-1017. [10.1016/j.cell.2007.10.050](#).
2. Pourmorady, A.D., Bashkirova, E.V., Chiariello, A.M., Belagzhal, H., Kodra, A., Duffie, R., Kahiapo, J., Monahan, K., Pulupa, J., Schieren, I., et al. (2024). RNA-mediated symmetry breaking enables singular olfactory receptor choice. *Nature* 625, 181-188. [10.1038/s41586-023-06845-4](#).
3. Dalton, R.P., Lyons, D.B., and Lomvardas, S. (2013). Co-opting the unfolded protein response to elicit olfactory receptor feedback. *Cell* 155, 321-332. [10.1016/j.cell.2013.09.033](#).
4. Shykind, B.M., Rohani, S.C., O'Donnell, S., Nemes, A., Mendelsohn, M., Sun, Y., Axel, R., and Barnea, G. (2004). Gene switching and the stability of odorant receptor gene choice. *Cell* 117, 801-815.

5. Serizawa, S., Miyamichi, K., Nakatani, H., Suzuki, M., Saito, M., Yoshihara, Y., and Sakano, H. (2003). Negative feedback regulation ensures the one receptor-one olfactory neuron rule in mouse. *Science* 302, 2088-2094. 10.1126/science.1089122
1089122 [pii].
6. Lewcock, J.W., and Reed, R.R. (2004). A feedback mechanism regulates monoallelic odorant receptor expression. *Proceedings of the National Academy of Sciences of the United States of America* 101, 1069-1074.
7. Shayya, H.J., Kahiapo, J.K., Duffie, R., Lehmann, K.S., Bashkurova, L., Monahan, K., Dalton, R.P., Gao, J., Jiao, S., Schieren, I., et al. (2022). ER stress transforms random olfactory receptor choice into axon targeting precision. *Cell*. 10.1016/j.cell.2022.08.025.
8. Wang, F., Nemes, A., Mendelsohn, M., and Axel, R. (1998). Odorant receptors govern the formation of a precise topographic map. *Cell* 93, 47-60.
9. Feinstein, P., Bozza, T., Rodriguez, I., Vassalli, A., and Mombaerts, P. (2004). Axon guidance of mouse olfactory sensory neurons by odorant receptors and the beta2 adrenergic receptor. *Cell* 117, 833-846. 10.1016/j.cell.2004.05.013
S0092867404005318 [pii].
10. Magklara, A., Yen, A., Colquitt, B.M., Clowney, E.J., Allen, W., Markenscoff-Papadimitriou, E., Evans, Z.A., Kheradpour, P., Mountoufaris, G., Carey, C., et al. (2011). An epigenetic signature for monoallelic olfactory receptor expression. *Cell* 145, 555-570. 10.1016/j.cell.2011.03.040.
11. Lyons, D.B., Magklara, A., Goh, T., Sampath, S.C., Schaefer, A., Schotta, G., and Lomvardas, S. (2014). Heterochromatin-mediated gene silencing facilitates the diversification of olfactory neurons. *Cell reports* 9, 884-892.
10.1016/j.celrep.2014.10.001.
12. Clowney, E.J., LeGros, M.A., Mosley, C.P., Clowney, F.G., Markenskoff-Papadimitriou, E.C., Myllys, M., Barnea, G., Larabell, C.A., and Lomvardas, S. (2012). Nuclear aggregation of olfactory receptor genes governs their monogenic expression. *Cell* 151, 724-737. 10.1016/j.cell.2012.09.043.
13. Le Gros, M.A., Clowney, E.J., Magklara, A., Yen, A., Markenscoff-Papadimitriou, E., Colquitt, B., Myllys, M., Kellis, M., Lomvardas, S., and Larabell, C.A. (2016). Soft X-Ray Tomography Reveals Gradual Chromatin Compaction and Reorganization during Neurogenesis In Vivo. *Cell reports* 17, 2125-2136. 10.1016/j.celrep.2016.10.060.
14. Lomvardas, S., Barnea, G., Pisapia, D.J., Mendelsohn, M., Kirkland, J., and Axel, R. (2006). Interchromosomal interactions and olfactory receptor choice. *Cell* 126, 403-413. 10.1016/j.cell.2006.06.035.
15. Markenscoff-Papadimitriou, E., Allen, W.E., Colquitt, B.M., Goh, T., Murphy, K.K., Monahan, K., Mosley, C.P., Ahituv, N., and Lomvardas, S. (2014). Enhancer interaction networks as a means for singular olfactory receptor expression. *Cell* 159, 543-557. 10.1016/j.cell.2014.09.033.
16. Monahan, K., Horta, A., and Lomvardas, S. (2019). LHX2- and LDB1-mediated trans interactions regulate olfactory receptor choice. *Nature* 565, 448-453. 10.1038/s41586-018-0845-0.
17. Pourmorady, A.D., Bashkurova, E.V., Chiariello, A.M., Belagzhal, H., Kodra, A., Duffie, R., Kahiapo, J., Monahan, K., Pulupa, J., Schieren, I., et al. (2023). RNA-mediated symmetry breaking enables singular olfactory receptor choice. *Nature*. 10.1038/s41586-023-06845-4.
18. Wu, H., Zhang, J., Jian, F., Chen, J.P., Zheng, Y., Tan, L., and Sunney Xie, X. (2024). Simultaneous single-cell three-dimensional genome and gene expression profiling uncovers dynamic enhancer connectivity underlying olfactory receptor choice. *Nat Methods*. 10.1038/s41592-024-02239-0.

19. Tan, L., Xing, D., Daley, N., and Xie, X.S. (2019). Three-dimensional genome structures of single sensory neurons in mouse visual and olfactory systems. *Nature structural & molecular biology* 26, 297-307. 10.1038/s41594-019-0205-2.
20. Bashkirova, E.V., Klimpert, N., Monahan, K., Campbell, C.E., Osinski, J., Tan, L., Schieren, I., Pourmorady, A., Stecky, B., Barnea, G., et al. (2023). Opposing, spatially-determined epigenetic forces impose restrictions on stochastic olfactory receptor choice. *eLife* 12. 10.7554/eLife.87445.
21. Lyons, D.B., Allen, W.E., Goh, T., Tsai, L., Barnea, G., and Lomvardas, S. (2013). An epigenetic trap stabilizes singular olfactory receptor expression. *Cell* 154, 325-336. 10.1016/j.cell.2013.06.039.
22. Imai, T., Suzuki, M., and Sakano, H. (2006). Odorant receptor-derived cAMP signals direct axonal targeting. *Science* 314, 657-661. 1131794 [pii] 10.1126/science.1131794.
23. Serizawa, S., Miyamichi, K., Takeuchi, H., Yamagishi, Y., Suzuki, M., and Sakano, H. (2006). A neuronal identity code for the odorant receptor-specific and activity-dependent axon sorting. *Cell* 127, 1057-1069. S0092-8674(06)01404-8 [pii] 10.1016/j.cell.2006.10.031.
24. Tan, L., Li, Q., and Xie, X.S. (2015). Olfactory sensory neurons transiently express multiple olfactory receptors during development. *Molecular systems biology* 11, 844. 10.15252/msb.20156639.
25. Hanchate, N.K., Kondoh, K., Lu, Z., Kuang, D., Ye, X., Qiu, X., Pachter, L., Trapnell, C., and Buck, L.B. (2015). Single-cell transcriptomics reveals receptor transformations during olfactory neurogenesis. *Science* 350, 1251-1255. 10.1126/science.aad2456.
26. Shum, E.Y., Espinoza, J.L., Ramaiah, M., and Wilkinson, M.F. (2015). Identification of novel post-transcriptional features in olfactory receptor family mRNAs. *Nucleic acids research* 43, 9314-9326. 10.1093/nar/gkv324.
27. Tan, K., Jones, S.H., Lake, B.B., Chousal, J.N., Shum, E.Y., Zhang, L., Chen, S., Sohni, A., Pandya, S., Gallo, R.L., et al. (2020). The role of the NMD factor UPF3B in olfactory sensory neurons. *eLife* 9. 10.7554/eLife.57525.
28. Buchet-Poyau, K., Courchet, J., Le Hir, H., Seraphin, B., Scoazec, J.Y., Duret, L., Domon-Dell, C., Freund, J.N., and Billaud, M. (2007). Identification and characterization of human Mex-3 proteins, a novel family of evolutionarily conserved RNA-binding proteins differentially localized to processing bodies. *Nucleic acids research* 35, 1289-1300. 10.1093/nar/gkm016.
29. Barriga, F.M., Montagni, E., Mana, M., Mendez-Lago, M., Hernando-Momblona, X., Sevillano, M., Guillaumet-Adkins, A., Rodriguez-Esteban, G., Buczacki, S.J.A., Gut, M., et al. (2017). Mex3a Marks a Slowly Dividing Subpopulation of Lgr5+ Intestinal Stem Cells. *Cell Stem Cell* 20, 801-816 e807. 10.1016/j.stem.2017.02.007.
30. Pereira, B., Amaral, A.L., Dias, A., Mendes, N., Muncan, V., Silva, A.R., Thibert, C., Radu, A.G., David, L., Maximo, V., et al. (2020). MEX3A regulates Lgr5(+) stem cell maintenance in the developing intestinal epithelium. *EMBO Rep* 21, e48938. 10.15252/embr.201948938.
31. Naef, V., De Sarlo, M., Testa, G., Corsinovi, D., Azzarelli, R., Borello, U., and Ori, M. (2020). The Stemness Gene Mex3A Is a Key Regulator of Neuroblast Proliferation During Neurogenesis. *Front Cell Dev Biol* 8, 549533. 10.3389/fcell.2020.549533.
32. Domingo-Muelas, A., Duart-Abadia, P., Morante-Redolat, J.M., Jordan-Pla, A., Belenguer, G., Fabra-Beser, J., Paniagua-Herranz, L., Perez-Villalba, A., Alvarez-Varela, A., Barriga, F.M., et al. (2023). Post-transcriptional control of a stemness signature by RNA-binding protein MEX3A regulates murine adult neurogenesis. *Nature communications* 14, 373. 10.1038/s41467-023-36054-6.

33. Lederer, M., Muller, S., Glass, M., Bley, N., Ihling, C., Sinz, A., and Huttelmaier, S. (2021). Oncogenic Potential of the Dual-Function Protein MEX3A. *Biology (Basel)* *10*. 10.3390/biology10050415.
34. Yu, C.R., Power, J., Barnea, G., O'Donnell, S., Brown, H.E., Osborne, J., Axel, R., and Gogos, J.A. (2004). Spontaneous neural activity is required for the establishment and maintenance of the olfactory sensory map. *Neuron* *42*, 553-566. S0896627304002247 [pii].
35. Nguyen, M.Q., Marks, C.A., Belluscio, L., and Ryba, N.J. (2010). Early expression of odorant receptors distorts the olfactory circuitry. *J Neurosci* *30*, 9271-9279. 10.1523/JNEUROSCI.1502-10.2010.
36. Hanke, T., Szawlowski, P., and Randall, R.E. (1992). Construction of solid matrix-antibody-antigen complexes containing simian immunodeficiency virus p27 using tag-specific monoclonal antibody and tag-linked antigen. *J Gen Virol* *73 (Pt 3)*, 653-660. 10.1099/0022-1317-73-3-653.
37. Kawaguchi, D., Sahara, S., Zembrzycki, A., and O'Leary, D.D.M. (2016). Generation and analysis of an improved Foxg1-IRES-Cre driver mouse line. *Developmental biology* *412*, 139-147. 10.1016/j.ydbio.2016.02.011.
38. Alvarez-Varela, A., Novellasdemunt, L., Barriga, F.M., Hernando-Momblona, X., Canellas-Socias, A., Cano-Crespo, S., Sevillano, M., Cortina, C., Stork, D., Morral, C., et al. (2022). Mex3a marks drug-tolerant persister colorectal cancer cells that mediate relapse after chemotherapy. *Nat Cancer* *3*, 1052-1070. 10.1038/s43018-022-00402-0.
39. Fleischmann, A., Shykind, B.M., Sosulski, D.L., Franks, K.M., Glinka, M.E., Mei, D.F., Sun, Y., Kirkland, J., Mendelsohn, M., Albers, M.W., and Axel, R. (2008). Mice with a "monoclonal nose": perturbations in an olfactory map impair odor discrimination. *Neuron* *60*, 1068-1081. 10.1016/j.neuron.2008.10.046.
40. Fleischmann, A., Abdus-Saboor, I., Sayed, A., and Shykind, B. (2013). Functional interrogation of an odorant receptor locus reveals multiple axes of transcriptional regulation. *PLoS biology* *11*, e1001568. 10.1371/journal.pbio.1001568.
41. Borden, K.L., Lally, J.M., Martin, S.R., O'Reilly, N.J., Solomon, E., and Freemont, P.S. (1996). In vivo and in vitro characterization of the B1 and B2 zinc-binding domains from the acute promyelocytic leukemia protooncogene PML. *Proceedings of the National Academy of Sciences of the United States of America* *93*, 1601-1606. 10.1073/pnas.93.4.1601.
42. McGlincy, N.J., and Ingolia, N.T. (2017). Transcriptome-wide measurement of translation by ribosome profiling. *Methods* *126*, 112-129. 10.1016/j.ymeth.2017.05.028.
43. Ingolia, N.T., Ghaemmaghami, S., Newman, J.R., and Weissman, J.S. (2009). Genome-wide analysis in vivo of translation with nucleotide resolution using ribosome profiling. *Science* *324*, 218-223. 10.1126/science.1168978.
44. Draper, B.W., Mello, C.C., Bowerman, B., Hardin, J., and Priess, J.R. (1996). MEX-3 is a KH domain protein that regulates blastomere identity in early *C. elegans* embryos. *Cell* *87*, 205-216. 10.1016/s0092-8674(00)81339-2.
45. Tirosh, I., Venteicher, A.S., Hebert, C., Escalante, L.E., Patel, A.P., Yizhak, K., Fisher, J.M., Rodman, C., Mount, C., Filbin, M.G., et al. (2016). Single-cell RNA-seq supports a developmental hierarchy in human oligodendroglioma. *Nature* *539*, 309-313. 10.1038/nature20123.
46. Weyn-Vanhenenryck, S.M., Feng, H., Ustianenko, D., Duffie, R., Yan, Q., Jacko, M., Martinez, J.C., Goodwin, M., Zhang, X., Hengst, U., et al. (2018). Precise temporal regulation of alternative splicing during neural development. *Nature communications* *9*, 2189. 10.1038/s41467-018-04559-0.
47. Heijmans, J., van Lidth de Jeude, J.F., Koo, B.K., Rosekrans, S.L., Wielenga, M.C., van de Wetering, M., Ferrante, M., Lee, A.S., Onderwater, J.J., Paton, J.C., et al. (2013). ER

- stress causes rapid loss of intestinal epithelial stemness through activation of the unfolded protein response. *Cell reports* 3, 1128-1139. 10.1016/j.celrep.2013.02.031.
48. Laguesse, S., Creppe, C., Nedialkova, D.D., Prevot, P.P., Borgs, L., Huysseune, S., Franco, B., Duysens, G., Krusy, N., Lee, G., et al. (2015). A Dynamic Unfolded Protein Response Contributes to the Control of Cortical Neurogenesis. *Developmental cell* 35, 553-567. 10.1016/j.devcel.2015.11.005.
49. Clowney, E.J., Magklara, A., Colquitt, B.M., Pathak, N., Lane, R.P., and Lomvardas, S. (2011). High-throughput mapping of the promoters of the mouse olfactory receptor genes reveals a new type of mammalian promoter and provides insight into olfactory receptor gene regulation. *Genome research* 21, 1249-1259. 10.1101/gr.120162.110.

Figure 1

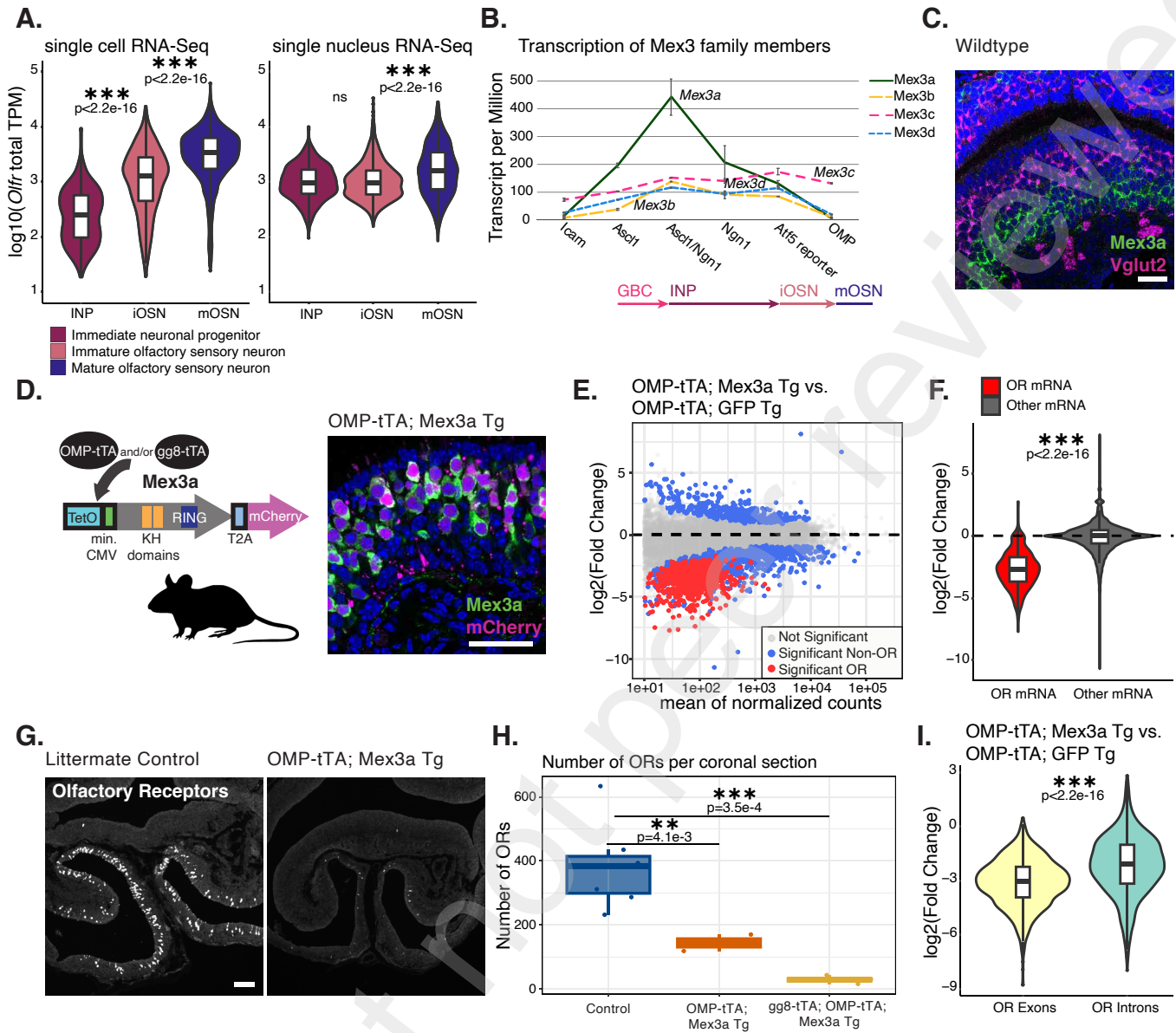


Figure 2

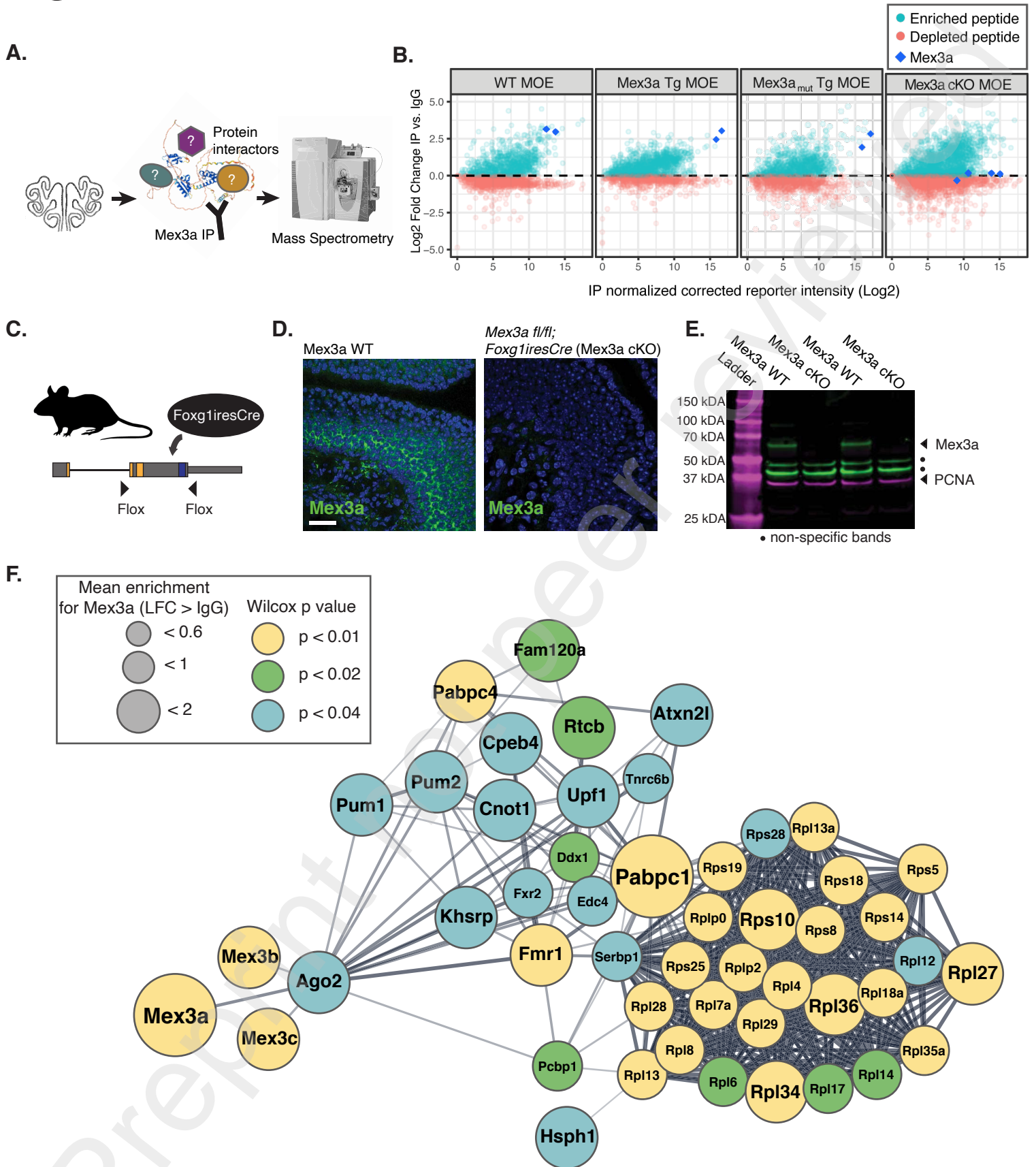


Figure 3

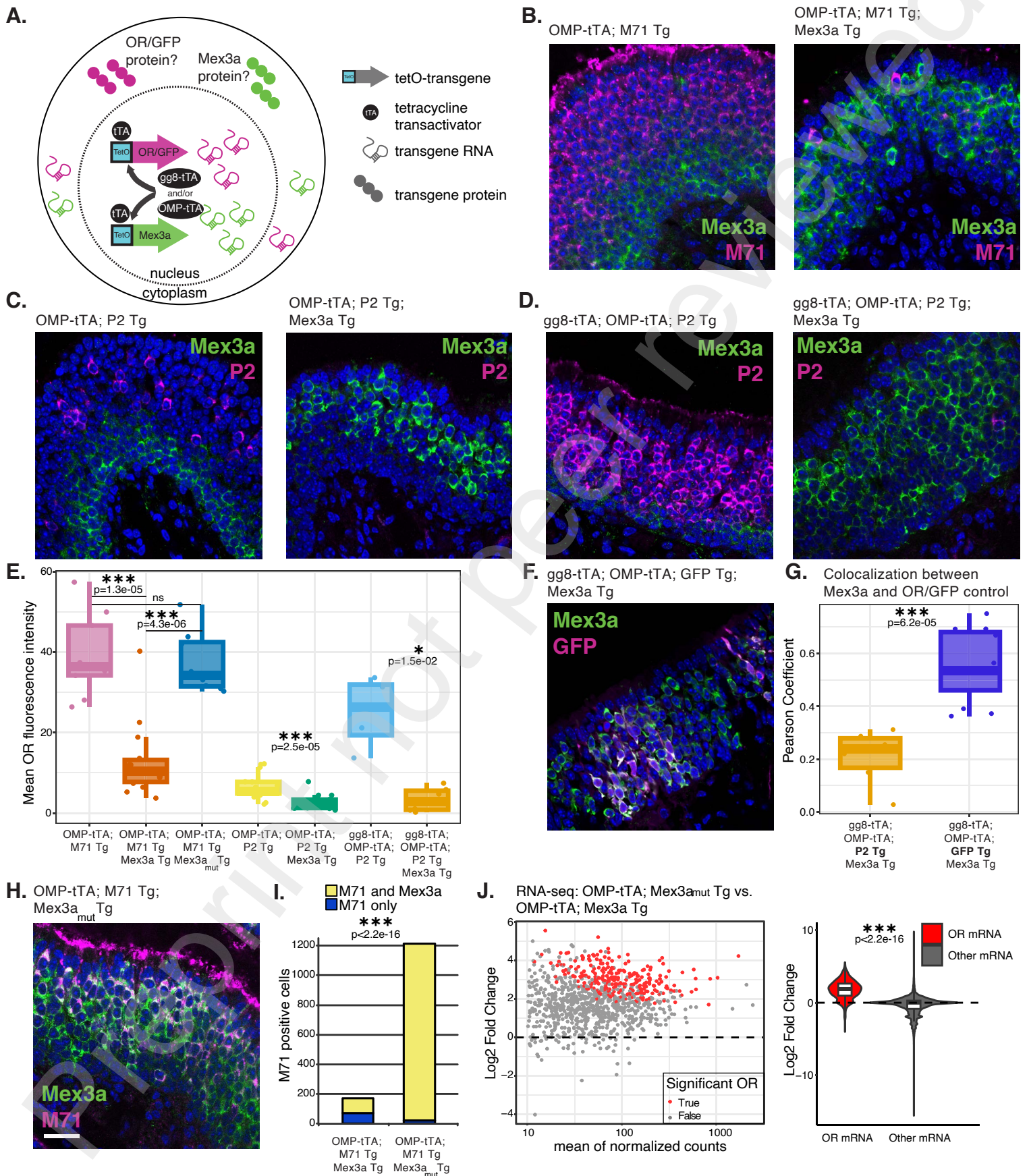
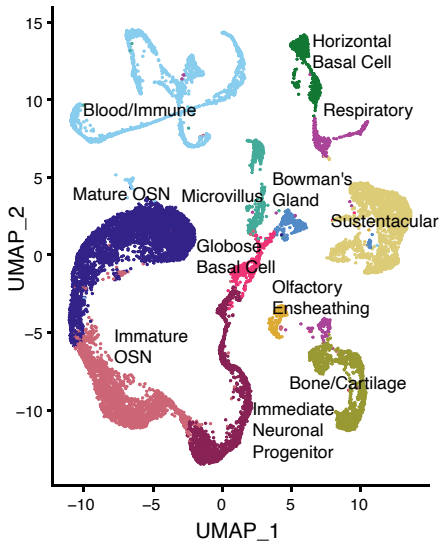
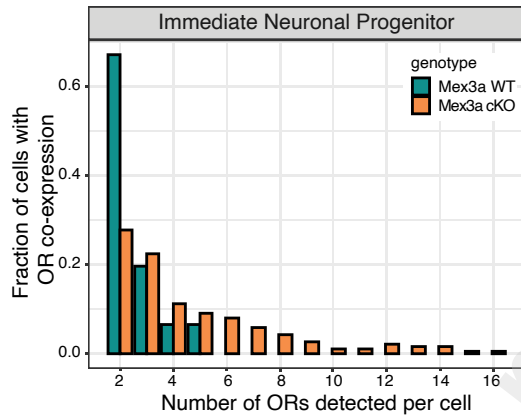


Figure 4

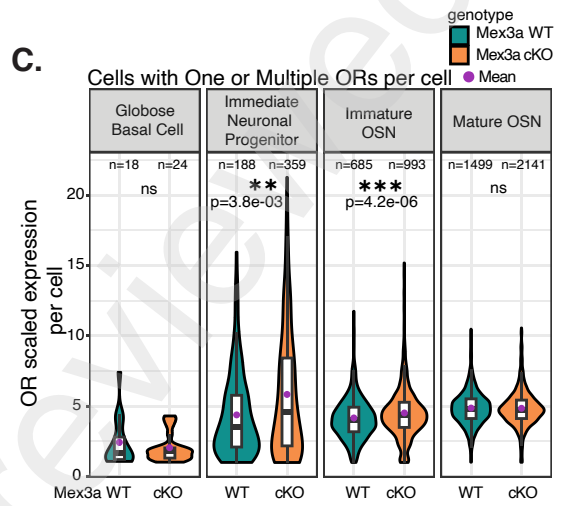
A.



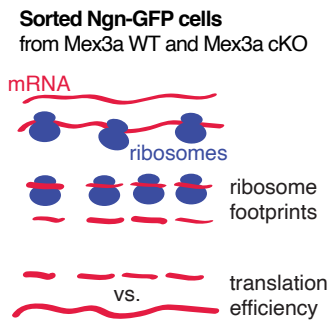
B.



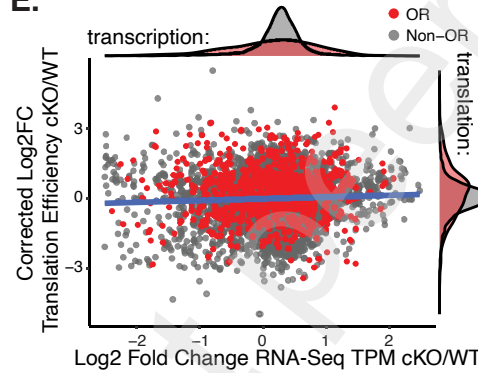
C.



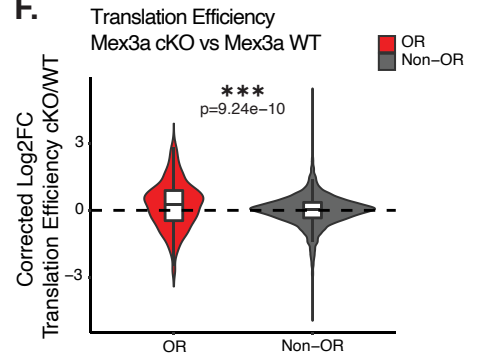
D.



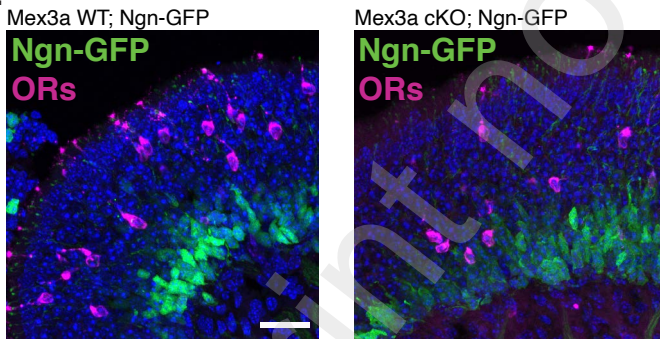
E.



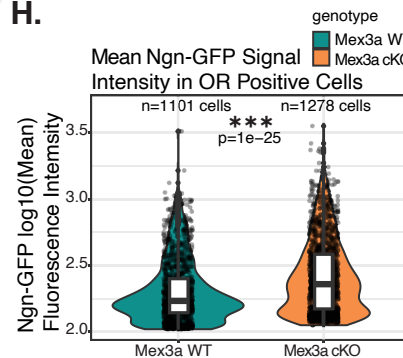
F.



G.



H.



I.

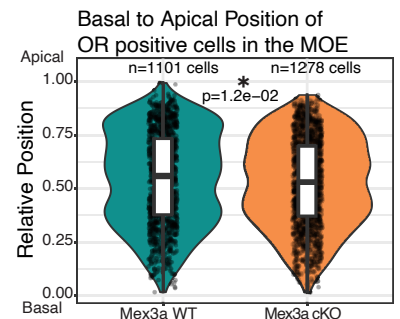


Figure 5

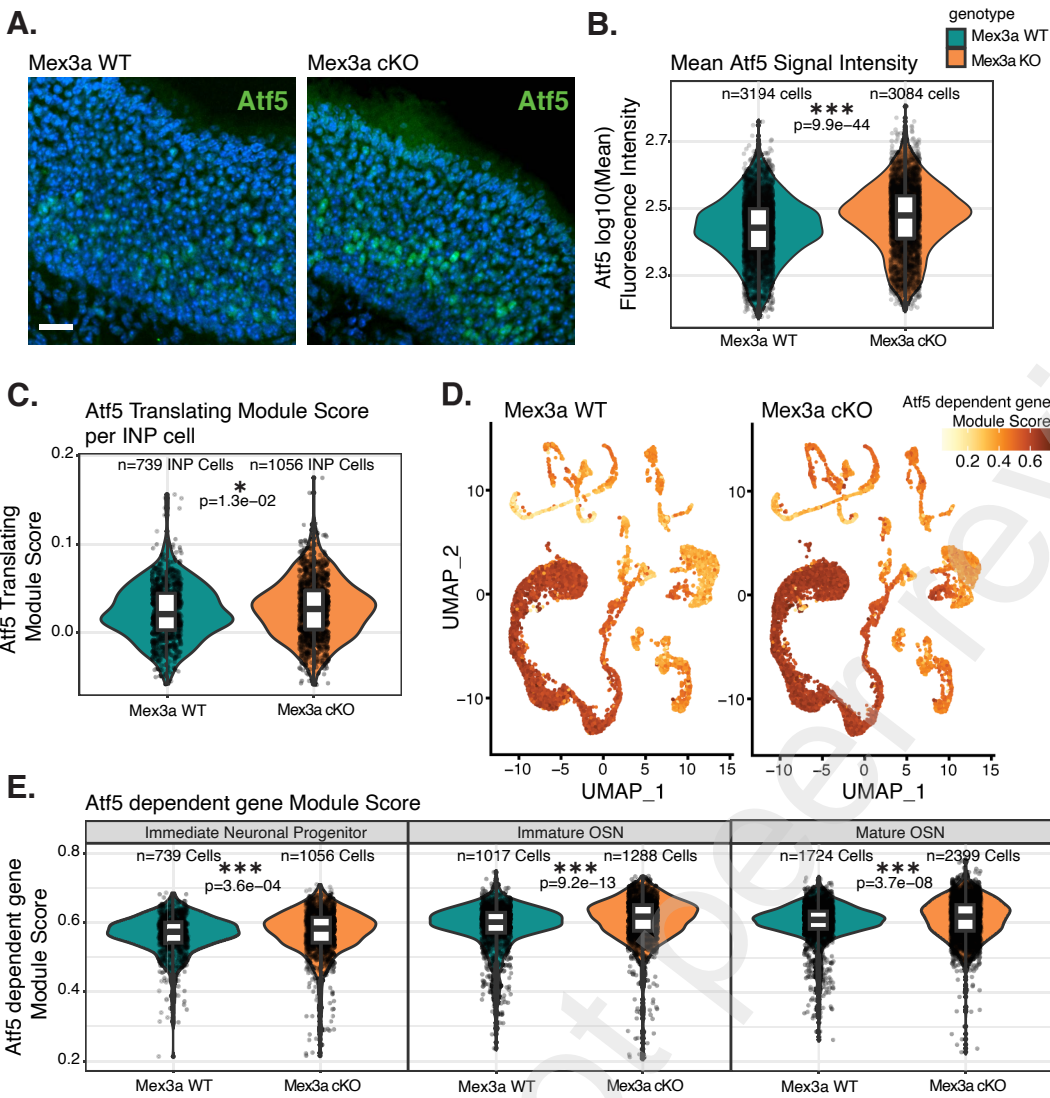


Figure 6

